Microscopic origin of magnetocrystalline anisotropy in transition metal thin films

1998 J. Phys.: Condens. Matter 10 3239

(http://iopscience.iop.org/0953-8984/10/14/012)

J. Phys.: Condens. Matter **10** (1998) 3239–3253. Printed in the UK PII: S0953-8984(98)86583-1

Microscopic origin of magnetocrystalline anisotropy in transition metal thin films

Gerrit van der Laan†

Daresbury Laboratory, Warrington WA4 4AD, UK

Received 4 August 1997, in final form 4 November 1997

Abstract. We investigate the relation between the magnetocrystalline anisotropy energy (MAE) and the electronic structure for transition metal thin films and surfaces which can display enhanced orbital magnetic moments. When the spin–orbit interaction is treated in second order, the MAE is proportional to the expectation value of the orbital magnetic moment as given by Bruno's model. However, there are additional terms which are related to the spin-subband orbital moment and to the magnetic dipole operator due to the anisotropy of the field of the spin. The latter term accounts for the spin-flip excitations between the exchange split majority and minority spin bands. A conjecture is proposed which relates the MAE to the expectation values of the orbital moments and the magnetic dipole term. It is shown how the different terms can be obtained experimentally with (transverse) magnetic circular x-ray dichroism. The model explains the experimentally observed perpendicular magnetic anisotropy in Co and Fe based multilayers and thin films.

1. Introduction

Conventional magnetism has ignored the anisotropy of the spin moment, and so far, not much is known about the factors which influence the magnetization of thin films, multilayers and interfaces. Yet the ability to grow thin epitaxial films has led to materials with novel magnetic properties, such as perpendicular magnetic anisotropy (PMA), giant magnetoresistance (GMR) and exchange biasing, with immediate technological applications. The preferred orientation of the magnetization is determined by the magnetocrystalline anisotropy energy (MAE), which is the change in the free energy for a crystal upon rotation of the magnetization. In thin films and multilayers the MAE is usually strongly different from the bulk due to the symmetry breaking. By varying the individual layer thickness and choice of the appropriate elements, it is possible to manipulate the magnetic anisotropy. A dramatic manifestation in this respect is the change of the preferential direction of the magnetization from the commonly observed in-plane orientation to the perpendicular direction [1, 2].

The exchange interaction is invariant for a rotation of the direction of the quantization axis of the spin, i.e. the magnetization direction. Therefore, the exchange interaction cannot explain the MAE. An interaction is required which couples the spins with the crystalline field. This would suggest that the MAE is due to the interatomic dipole–dipole interaction between the spins, which lead to a macroscopic shape anisotropy that is proportional to the

† Fax: 01925-603124. E-mail address: g.vanderlaan@dl.ac.uk

0953-8984/98/143239+15$19.50

square of the saturation value of the magnetization [3]. Calculations of the surface shape anisotropy, however, show that this contribution is several orders too small to explain the experimental results [3–5], and that other sources of anisotropy are apparently dominant. In any case the surface shape anisotropy cannot explain the PMA observed in thin films.

Van Vleck [6] attributed the physical origin of the MAE to the spin–orbit coupling. This interaction can be interpreted as the coupling between the spin of the electron and the magnetic field created by its own orbital motion around the nucleus. The orbital motion is coupled to the lattice via the electric potential of the ions. The spin–orbit interaction is large in the neighbourhood of the nucleus, where the potential is spherical symmetric, so that it can be considered as a localized interaction.

The ideas of Van Vleck were extended to itinerant ferromagnets by Brooks [7] using a semi-empirical band structure model. Only recently *ab initio* relativistic Dirac calculations have been used to obtain the MAE of transition metals [8]. However, such calculations are not reliable for cubic transition metals, where the small value for the MAE, in the order of μeV, is obtained by subtracting two large numbers, in the order of eV, for the total energies of the different magnetization directions. First-principles calculations in the local density approximation (LSDA) have predicted a wrong easy direction in Co and Ni metal [9]. Even at surfaces and interfaces where the MAE is an order of magnitude larger, these calculations are not completely reliable. Also for the orbital moment the situation is unsatisfactory. For Ni the theoretical value agrees with experiment, but for Fe and Co they are roughly half the experimental values. Including the orbital polarization term adopted from atomic theory results in a correct value of the orbital moment for Co and Fe, but a value twice too large for Ni metal. A further problem is that the number of k points in the calculation has to be very large in order to obtain a stable result for the MAE [10]. Therefore, Wang *et al* [11] proposed the so-called state-tracking method, which avoids regions in k space where the orbital moment is degenerate, because their first-order contribution can lead to large fluctuations in the calculated MAE as a function of band filling. Daalderop *et al* [12] have argued that this method is unjustified and even unnecessary.

We will investigate the situation where the spin–orbit interaction is small compared to the bandwidth. In 3d transition metals the spin–orbit constant is between 40 and 80 meV [13], which is small compared with the bandwidth of a few eV, so that in this case a perturbative treatment is justified. For rare earths the situation is completely different and the reader is referred to [14] and [15]. Using perturbation theory Bruno [16] showed how the dependence on the electronic structure can be separated from the angular dependence. The latter dependence has been discussed in detail in [17] and [18]. The separation makes it possible to calculate the different anisotropy constants directly from the unperturbed band structure [19]. The advantage of perturbation theory is that it allows to calculate directly the anisotropy constants without calculating explicitly the total energy of the system as a function of the direction of the magnetization. However, it does not take into account any changes of the Fermi surface. Bruno [16] showed that if the majority spin band is completely filled the MAE is proportional to the orbital magnetization. Wang *et al* [20] showed that there is also an additional contribution to the MAE due to a spin-flip term, which can be related to the quadrupole moment of the ground state.

The spin and orbital magnetic moment and the magnetic dipole term of the ground state are given by the expectation values of the vector operators $\boldsymbol{S}$, $\boldsymbol{L}$ and $\boldsymbol{T}$, respectively [21]. Similarly, the charge density and its anisotropy are determined by the expectation values of the number of holes, n_h, and the quadrupole moment, $\boldsymbol{Q}$, respectively [22]. $\boldsymbol{T}$ is due to the anisotropy in the spin moment, which can be induced either by an anisotropic charge distribution or by spin–orbit interaction. Although the spin anisotropy is a fundamental

part of the description of the electronic ground state, it does not contribute to the magnetic moment as measured by more traditional techniques which are relying on the isotropic exchange interaction. However, physical properties, such as the MAE, will depend on the anisotropy in both the orbital magnetic moment and the spin moment. The value of $\boldsymbol{T}$, which is small in cubic systems, can be strongly enhanced at surfaces and interfaces due to symmetry breaking. Its expectation value will also be larger in 4d and 5d transition metals compared to 3d transition metals, because $\boldsymbol{T}$ contains a contribution which depends on the magnitude of the spin–orbit interaction, as has been observed in the case of actinides, where $\boldsymbol{T}$ can exceed the value of $\boldsymbol{L}$ [23, 24]. We will outline how these different moments can be obtained experimentally in section 4.2, after we have established in section 3 which of these quantities are important from theoretical perspective.

Magnetic moments at the surface and in thin films and interfaces are often, but not always, enhanced. A simple reason for this is the reduced coordination number at the surface, which results in a narrowing of the d band width [25]. A large enhancement in the spin magnetic moments of 3d transition metal surfaces has been predicted by band structure models [26]. Only recently it was realized that also the orbital magnetic moment can be strongly enhanced. The first experimental evidence was obtained by van der Laan *et al* [27], who observed an enhancement of the orbital moment for a Ni(110) surface using magnetic circular dichroism in photoemission at the Ni 2p core level. More recently, enhanced orbital moments were also observed with MCXD for Co on Cu(100) by Tischer *et al* [28] and for Co-based nanostructures by Dürr *et al* [29].

Various reasons have been put forward to explain the enhancement of the orbital moment at the surface:

(i) At the surface the d band is narrower, resulting in an increase of the spin magnetic moment. The spin–orbit interaction couples the orbit to the spin moment, so that the orbital magnetic moment will increase with the spin magnetic moment [30].

(ii) The symmetry is reduced at the surface, which can remove the quenching of the orbital moment, that often occurs in high lattice symmetries, such as cubic structures.

(iii) The density of states at the Fermi level can be larger than in the bulk, increasing the orbital magnetic moment.

(iv) Surface roughness, interdiffusion, steps and terraces increase the electron localization, leading to more localized atomic wavefunction with increased orbital moments compared to the bulk.

(v) Thin films can give a confinement of the electronic wavefunction leading to symmetry breaking and localization.

(vi) Thin films can show a strain-induced anisotropy due to the lattice mismatch of the substrate, which breaks the lattice symmetry of the film. An example is Ni/Cu(001) which shows PMA between 7 and 56 ML. It grows pseudomorphic with $\sim$2.5% elongated Ni–Ni distance in plane and a reduced layer spacing normal to the surface, i.e. an artificial structure with face-centred tetragonal (fct) symmetry is created. In the fct structure the orbital moment is no longer quenched.

In this paper we are particularly interested in the origin of the MAE at the surface and in thin films and multilayers. In section 2 we will first discuss the orbital degeneracy, which is important in order to understand the symmetry aspects involved in the problem. We also show using general symmetry arguments that an exact expression for the MAE in terms of magnetic ground state moments cannot be obtained. In section 3 we give a derivation of the different terms appearing in the expression of the MAE. We extend the model given by Bruno by including the majority spin band orbital moment and spin-flip excitations.

A discussion is given in section 4, where we show how the different terms can be obtained experimentally with (transverse) magnetic circular x-ray dichroism and we present a phase diagram for the magnetic preference of a thin film. Conclusions are drawn in section 5.

2. Orbital degeneracy

Van Vleck [31, 32] has already showed for a free ion that the absence of orbital degeneracy is a sufficient condition for the quenching of the orbital moment, which means that the first-order contribution should vanish: $\langle\Psi|L_\zeta|\Psi\rangle = 0$. This can be seen as follows. Let Ψ be a non-degenerate eigenstate of the system. When spin-dependent interactions can be neglected, the Hamiltonian H will be a real operator. We can then assume that Φ is real, because if it was complex of the form $\psi_1 + \mathrm{i}\psi_2$ and H real, ψ_1 and ψ_2 would be separately eigenfunctions of H with the same energy and the level would be degenerate, in contradiction with the initial assumption. However, the angular momentum operator, $\boldsymbol{L}$, is purely imaginary, so that the expectation value of any of its components taken over a real wavefunction is imaginary. On the other hand, since $\boldsymbol{L}$ is Hermitian, this expectation value must be real, therefore, it must vanish. The quenching of the orbital moment shows that the influence of the surroundings is of prime importance on the magnetic properties of an ion, and that there is a close connection between magnetism and degeneracy. The rotational symmetry in a free ion corresponds to a degeneracy, which, in a lower symmetry, may be lifted partially or totally, resulting in a change of the magnetic properties of the ion.

An electron in a particular orbital will have an orbital angular momentum along a given axis, when by rotation about that axis, the orbital can be transformed into an equivalent and degenerate orbital which does not contain an electron with the same spin [33]. Such a transformation will allow the electron to rotate about the axis, i.e. the electron has an orbital moment along the axis. For instance, a rotation of 45° about the z axis will turn the xy orbital into the $x^2 - y^2$ orbital, whereas a rotation of 90° changes the xy orbital into the yz orbital. Thus one would expect an orbital moment from an electron in either of these pairs of orbitals. The $3z^2 - r^2$ cannot be transformed into any of the other orbitals by a rotation about the z axis, thus will not give an orbital moment in the z direction. A cubic crystal field removes the degeneracy of the d orbitals, resulting in representations T_2 (xy, yz and zx) and E ($3z^2 - r^2$ and $x^2 - y^2$), which are separated in energy by the crystal field parameter Δ. The degeneracy of the xy and $x^2 - y^2$ orbitals is destroyed, and, in second order, the orbital contribution is reduced by a factor $2\xi/\Delta$, where ξ is the spin–orbit parameter ($\xi \ll \Delta$). Because the $3z^2 - r^2$ and $x^2 - y^2$ orbitals cannot be transformed into each other by rotation about any axis, the E representation can have no orbital moment. However, the zx and yz orbitals are still degenerate and can give an orbital moment. Thus a crystal field gives a reduction of the orbital moment depending on its symmetry and strength.

The symmetry aspects involved in the quenching of the orbital moment can also be captured by a more general rule. Once we know the behaviour of a certain operator in spherical symmetry (SO_3), the influence of the crystal field can be determined using the Wigner–Eckart theorem [34]. In spherical symmetry the matrix element $\langle LSJ|l^x s^y j^z|L'S'J'\rangle$ of a coupled operator $l^x s^y j^z$ is non-zero only if

$$C(LxL')C(SyS')C(JzJ') \neq 0 \tag{1}$$

where $C(lkm)$ is the $3j$ factor of the irreps k, l and m in the chosen symmetry group, which is only non-zero when the Kronecker product over the three irreps exists. Therefore, $C(LxL')$, $C(SyS')$ and $C(JzJ')$ must be non-zero, which results in the selection rules $\Delta L = 0, \pm x$, $\Delta S = 0, \pm y$ and $\Delta J = 0, \pm z$.

For the orbital moment operator we have $x = 1$, $y = 0$ and $z = 1$. In a basis ΓS, where 1 branches to the representation γ, a matrix element is non-zero when $C(\Gamma\gamma\Gamma')$ contains the totally symmetric representation. The first-order interaction is given by the diagonal matrix elements, where the Kronecker products $\Gamma \times \Gamma$ must contain γ. In the group C_s, C_n, C_{nh} and S_{2n} the set of γ contains the totally symmetric representation, so that this condition is met for all terms. In the cubic group the diagonal elements of the orbital momentum operator vanish only for the representation E, since $E \times T_1 \times E$ has no totally symmetric component.

The MAE is determined by the spin–orbit interaction with $x = 1$, $y = 1$ and $z = 0$, so that the orbital selection rule is the same as for the orbital moment operator, but the spin selection rule is relaxed, allowing for spin-flip transitions. Whereas the spin–orbit operator is a scalar, the orbital moment operator is represented by an axial vector, which changes sign under time reversal. Differences in symmetry between the ground state operators prohibit writing down a exact relation, so that—at best—only an approximate relation can be postulated.

3. Theory

3.1. Ground state properties

A few remarks about the properties of the ground state are in order to understand the following theory [21]. The main purpose of this section is to derive for itinerant transition metals a conjecture which relates the MAE with the expectation values of the ground state moments $\boldsymbol{L}$ and $\boldsymbol{T}$. First we will derive expressions for the second-order spin–orbit contribution of both the MAE and the orbital magnetic moment. We shall see that the MAE contains a spin-flip term which cannot be described by the orbital moment operator since the latter does not act on the spin. We therefore postulate a term proportional to $\boldsymbol{T}$ which can account for most of the remaining MAE. Since the energy is a scalar the moments in the expression will enter as $\hat{\boldsymbol{S}} \cdot \boldsymbol{L}$ and $\hat{\boldsymbol{S}} \cdot \boldsymbol{T}$, where $\hat{\boldsymbol{S}}$ is the magnetization direction which is along the unit vector of the spin magnetic moment, $\hat{\boldsymbol{S}} = \boldsymbol{S}/S$. This is possible because $\boldsymbol{S}$ represents the isotropic spin distribution. The anisotropic part of the spin distribution is given by $\boldsymbol{T} = \hat{\boldsymbol{S}} - 3\hat{\boldsymbol{r}}(\hat{\boldsymbol{r}} \cdot \boldsymbol{S})$, where $\hat{\boldsymbol{r}}$ is the position unit vector [35, 36]. When the spin–orbit coupling is small we can write [37]

$$\boldsymbol{T} \approx -\tfrac{2}{7}\boldsymbol{Q} \cdot \hat{\boldsymbol{S}} \tag{2}$$

where $\boldsymbol{Q}$ is the quadrupole moment of the charge distribution

$$\boldsymbol{Q} = \boldsymbol{L}^2 - \tfrac{1}{3}L^2 \tag{3}$$

which is a traceless spherical tensor of rank 2.

3.2. Electronic structure

We consider a d band metal with eigenfunctions $|\boldsymbol{k}, n, \sigma\rangle$ and eigenvalues $\varepsilon_{n,\sigma}(\boldsymbol{k})$ as the Fourier transform of the Bloch functions $|\boldsymbol{k}, \mu, \sigma\rangle$

$$|\boldsymbol{k}, n, \sigma\rangle = \sum_{\mu} a_{n,\mu,\sigma}(\boldsymbol{k})|\boldsymbol{k}, \mu, \sigma\rangle \tag{4}$$

where $\boldsymbol{k}$ is the electron wave vector, μ represents the d orbitals $\{xy, yz, zx, x^2-y^2, 3z^2-r\}$ and σ is the spin.

The density of states for the state with spin σ is

$$n_{\mu,\underline{\mu},\sigma}(\boldsymbol{k},\varepsilon)=\sum_{n}a^{*}_{n,\underline{\mu},\sigma}(\boldsymbol{k})a_{n,\mu,\sigma}(\boldsymbol{k})\delta(\varepsilon-\varepsilon_{n,\sigma}(\boldsymbol{k})) \tag{5}$$

where we used two different orbitals indices, μ and $\underline{\mu}$, to allow for orbital degeneracy. The intra-atomic spin–orbit interaction is given by

$$H_{\rm so}=\xi\sum_{\mu_1,\mu_2,\sigma_1,\sigma_2}\langle\mu_2,\sigma_2|\boldsymbol{L}\cdot\boldsymbol{S}|\mu_1,\sigma_1\rangle\sum_{\boldsymbol{k}}c^{\dagger}_{\mu_2,\sigma_2}(\boldsymbol{k})c_{\mu_1,\sigma_1}(\boldsymbol{k}) \tag{6}$$

where $c^{\dagger}$ and c are creation and annihilation operators, respectively. $\xi\equiv\xi(\boldsymbol{r})$ is the radial part of the spin–orbit interaction. Because $H_{\rm so}$ is a one-electron operator diagonal in $\boldsymbol{k}$, the only excited states that have to be considered are those that couple to the ground state with

$$|{\rm ex}\rangle=c^{\dagger}_{n_2,\sigma_2}(\boldsymbol{k})c_{n_1,\sigma_1}(\boldsymbol{k})|{\rm gr}\rangle \tag{7}$$

where the subscripts 1 and 2 refer to the occupied and unoccupied states, respectively, and

$$\varepsilon_{n_1,\sigma_1}(\boldsymbol{k})<\varepsilon_{\rm F}<\varepsilon_{n_2,\sigma_2}(\boldsymbol{k}) \tag{8}$$

with $\varepsilon_{\rm F}$ the Fermi level.

3.3. MAE

The second-order contribution to the energy is

$$\delta E=\sum_{\rm ex}\frac{\langle{\rm gr}|H_{\rm so}|{\rm ex}\rangle\langle{\rm ex}|H_{\rm so}|{\rm gr}\rangle}{E_{\rm gr}-E_{\rm ex}}. \tag{9}$$

Substitution of

$$\sum_{\rm ex}|{\rm ex}\rangle\langle{\rm ex}|=\sum_{\boldsymbol{k},n_1,\sigma_1,n_2,\sigma_2}c^{\dagger}_{n_2,\sigma_2}(\boldsymbol{k})c_{n_1,\sigma_1}(\boldsymbol{k})|{\rm gr}\rangle\langle{\rm gr}|c^{\dagger}_{n_1,\sigma_1}(\boldsymbol{k})c_{n_2,\sigma_2}(\boldsymbol{k})| \tag{10}$$

together with (6) into (9) and introducing the shorthand notation $\theta=\mu_1,\underline{\mu}_1,\mu_2,\underline{\mu}_2$ to define

$$A(\theta,\sigma_1,\sigma_2)\equiv\int_{\varepsilon_1<\varepsilon_{\rm F}<\varepsilon_2}\frac{{\rm d}\varepsilon_1\,{\rm d}\varepsilon_2}{\varepsilon_2-\varepsilon_1}\sum_{\boldsymbol{k}}n_{\mu_1,\underline{\mu}_1,\sigma_1}(\boldsymbol{k},\varepsilon_1)n_{\mu_2,\underline{\mu}_2,\sigma_2}(\boldsymbol{k},\varepsilon_2) \tag{11}$$

we obtain

$$\begin{aligned}\delta E=-\xi^2\sum_{\theta}[&A(\theta,\uparrow,\uparrow)\langle\underline{\mu}_1,\uparrow|\boldsymbol{L}\cdot\boldsymbol{S}|\underline{\mu}_2,\uparrow\rangle\langle\mu_2,\uparrow|\boldsymbol{L}\cdot\boldsymbol{S}|\mu_1,\uparrow\rangle\\&+A(\theta,\downarrow,\downarrow)\langle\underline{\mu}_1,\downarrow|\boldsymbol{L}\cdot\boldsymbol{S}|\underline{\mu}_2,\downarrow\rangle\langle\mu_2,\downarrow|\boldsymbol{L}\cdot\boldsymbol{S}|\mu_1,\downarrow\rangle\\&-A(\theta,\uparrow,\downarrow)\langle\underline{\mu}_1,\uparrow|\boldsymbol{L}\cdot\boldsymbol{S}|\underline{\mu}_2,\downarrow\rangle\langle\mu_2,\downarrow|\boldsymbol{L}\cdot\boldsymbol{S}|\mu_1,\uparrow\rangle\\&-A(\theta,\downarrow,\uparrow)\langle\underline{\mu}_1,\downarrow|\boldsymbol{L}\cdot\boldsymbol{S}|\underline{\mu}_2,\uparrow\rangle\langle\mu_2,\uparrow|\boldsymbol{L}\cdot\boldsymbol{S}|\mu_1,\downarrow\rangle]\end{aligned} \tag{12}$$

which gives the energy contribution as a sum over terms which are split in a factor that depends on the occupation numbers and energies of the spin orbitals and an angular factor containing the matrix elements.

The energy gain can be visualized as caused by virtual excitations from a degenerate occupied level with spin σ_1 and orbitals characters μ_1 and $\underline{\mu}_1$ to an unoccupied level with spin σ_2 and orbital characters μ_2 and $\underline{\mu}_2$. Figure 1 gives a graphical representation for such a second-order excitation.

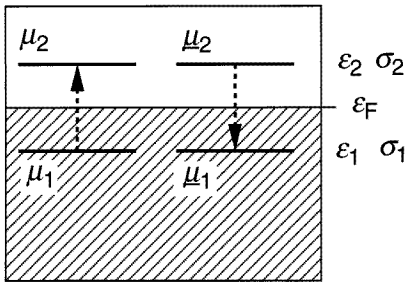

Figure 1. Graphical representation of the second-order contribution to the MAE due to virtual excitations from a degenerate occupied level with spin σ_1 and orbital characters μ_1 and $\underline{\mu}_1$ to an unoccupied level with spin σ_2 and orbital characters μ_2 and $\underline{\mu}_2$. The arrows are pointed towards the conjugate states.

3.4. Orbital moment

We can write the expectation value of the orbitals magnetic moment in second-order perturbation theory as

$$\langle \boldsymbol{L} \rangle = \sum_{\mathrm{ex}} \frac{\langle \mathrm{gr}|\boldsymbol{L}|\mathrm{ex}\rangle\langle \mathrm{ex}|H_{\mathrm{so}}|\mathrm{gr}\rangle}{E_{\mathrm{gr}} - E_{\mathrm{ex}}} \tag{13}$$

where the orbital moment operator is

$$\boldsymbol{L} = 4 \sum_{\mu_1,\mu_2,\sigma,\zeta} \langle \mu_2|\boldsymbol{L}_\zeta|\mu_1\rangle \sum_{\boldsymbol{k}} c^\dagger_{\mu_2,\sigma}(\boldsymbol{k}) c_{\mu_1,\sigma}(\boldsymbol{k}). \tag{14}$$

Because $\boldsymbol{L}$ does not change the spin, only excited states with the same spin can be reached, therefore in the scalar product

$$\boldsymbol{L}\cdot\boldsymbol{S} = L_\zeta S_\zeta + \tfrac{1}{2}(L_+ S_- + L_- S_+) \tag{15}$$

contained in H_{so} only the term $L_\zeta S_\zeta$ will survive. Equation (13) can then be written as

$$\begin{aligned}\langle \boldsymbol{L} \rangle &= -4\xi \sum_{\theta,\sigma} A(\theta,\sigma,\sigma)\langle \underline{\mu}_1|\boldsymbol{L}|\underline{\mu}_2\rangle\langle \mu_2|\boldsymbol{L}|\mu_1\rangle\langle \sigma|\boldsymbol{S}|\sigma\rangle \\ &= -4\xi \sum_{\theta}[A(\theta,\uparrow,\uparrow) - A(\theta,\downarrow,\downarrow)]\langle \underline{\mu}_1|\boldsymbol{L}_1|\underline{\mu}_2\rangle\langle \mu_2|\boldsymbol{L}|\mu_1\rangle\cdot\hat{\boldsymbol{S}}\end{aligned} \tag{16}$$

so that the orbital moment projected on the magnetization direction becomes

$$\begin{aligned}\hat{\boldsymbol{S}}\cdot\langle \boldsymbol{L}\rangle = -4\xi \sum_{\theta}[&A(\theta,\uparrow,\uparrow)\langle \underline{\mu}_1,\uparrow|\boldsymbol{L}\cdot\boldsymbol{S}|\underline{\mu}_2,\uparrow\rangle\langle \mu_2,\uparrow|\boldsymbol{L}\cdot\boldsymbol{S}|\mu_1,\uparrow\rangle \\ &-A(\theta,\downarrow,\downarrow)\langle \underline{\mu}_1,\downarrow|\boldsymbol{L}\cdot\boldsymbol{S}|\underline{\mu}_2,\downarrow\rangle\langle \mu_2,\downarrow|\boldsymbol{L}\cdot\boldsymbol{S}|\mu_1,\downarrow\rangle]\end{aligned} \tag{17}$$

which can be compared with the expression for the MAE in (12). If we neglect the spin-flip terms we find

$$\delta E \approx -\tfrac{1}{4}\xi\hat{\boldsymbol{S}}\cdot[\langle \boldsymbol{L}^\downarrow\rangle - \langle \boldsymbol{L}^\uparrow\rangle] = -\tfrac{1}{4}\xi\hat{\boldsymbol{S}}\cdot[\langle \boldsymbol{S}\rangle - 2\langle \boldsymbol{L}^\uparrow\rangle] \tag{18}$$

where $\boldsymbol{L}^{\downarrow(\uparrow)}$ is the orbital moment vector of the spin down (up) band. If we assume that the majority spin ($\uparrow$) band is completely filled, as in Bruno's model [16], its orbital moment vanishes and we obtain that δE is directly proportional to $\langle \boldsymbol{L}\rangle$. For metals with a nearly filled band this might often account for the main contribution to the MAE; however, in general the three other terms in (12) cannot be ignored.

3.5. Spin-flip excitations

Whereas in the case of $\boldsymbol{L}$ we are primarily concerned with low-energy excitations which conserve the spin moment, the MAE also contains terms where the spin, σ_2, of the excited state is reversed compared to σ_1. Such a spin-flip term cannot be described by an orbital operator, which leaves the spin untouched. Therefore, it seems appropriate to postulate a term proportional to $\boldsymbol{T}$ which will account for most of the remaining MAE. When the spin–orbit interaction is small, the two spin bands are separated by the exchange splitting $\Delta E_{\rm ex}$. For large $\Delta E_{\rm ex} \equiv \varepsilon_2 - \varepsilon_1$ we can write

$$\frac{\langle {\rm gr}|H^2|{\rm gr}\rangle}{\Delta E_{\rm ex}} = \frac{1}{\Delta E_{\rm ex}} \sum_{\rm ex} \langle {\rm gr}|H|{\rm ex}\rangle\langle {\rm ex}|H|{\rm gr}\rangle$$
$$= \int_{\varepsilon_2>\varepsilon_{\rm F}} {\rm d}\varepsilon_2 \sum_{\boldsymbol{k},\mu_2,\underline{\mu}_2} n_{\mu_2,\underline{\mu}_2,\sigma_2}(\boldsymbol{k},\varepsilon_2) \frac{\langle {\rm gr}|H|\underline{\mu}_2,\sigma_2\rangle\langle\mu_2,\sigma_2|H|{\rm gr}\rangle}{\Delta E_{\rm ex}}. \tag{19}$$

We further define

$$n_{\mu_1,\underline{\mu}_1,\sigma_1} \equiv \int_{\varepsilon_1<\varepsilon_{\rm F}} {\rm d}\varepsilon_1 \sum_{\boldsymbol{k}} n_{\mu_1,\underline{\mu}_1,\sigma_1}(\boldsymbol{k},\varepsilon_1) \tag{20}$$

as the number of electrons in the ground state with indicated orbital and spin characters. For $H^2 = \hat{\boldsymbol{S}}\cdot\langle\boldsymbol{T}\rangle$ we can write using (2), (3), (19) and (20)

$$\hat{\boldsymbol{S}}\cdot\langle\boldsymbol{T}\rangle \approx -\frac{2}{7}\hat{\boldsymbol{S}}\cdot\langle\boldsymbol{Q}\rangle\cdot\hat{\boldsymbol{S}} = \frac{2}{21}\sum_{\mu_1,\underline{\mu}_1,\sigma_1} n_{\mu_1,\underline{\mu}_1,\sigma_1}\langle\underline{\mu}_1|\boldsymbol{L}^2 - 3(\boldsymbol{L}\cdot\boldsymbol{S})^2|\mu_1\rangle$$
$$= \frac{2}{21}\sum_{\mu_1,\underline{\mu}_1,\sigma_1} n_{\mu_1,\underline{\mu}_1,\sigma_1}[\langle\underline{\mu}_1|\boldsymbol{L}|\underline{\mu}_2\rangle\langle\mu_2|\boldsymbol{L}|\mu_1\rangle - 3\hat{\boldsymbol{S}}\cdot\langle\underline{\mu}_1|\boldsymbol{L}|\underline{\mu}_2\rangle\langle\mu_2|\boldsymbol{L}|\mu_1\rangle\cdot\hat{\boldsymbol{S}}]$$
$$= \frac{2}{21}\Delta E_{\rm ex}\sum_{\theta}[A(\theta,\uparrow,\downarrow)\langle\underline{\mu}_1,\uparrow|\boldsymbol{L}\cdot\boldsymbol{S}|\underline{\mu}_2,\downarrow\rangle\langle\mu_2,\downarrow|\boldsymbol{L}\cdot\boldsymbol{S}|\mu_1,\uparrow\rangle$$
$$+A(\theta,\downarrow,\uparrow)\langle\underline{\mu}_1,\downarrow|\boldsymbol{L}\cdot\boldsymbol{S}|\underline{\mu}_2,\uparrow\rangle\langle\mu_2,\uparrow|\boldsymbol{L}\cdot\boldsymbol{S}|\mu_1,\downarrow\rangle$$
$$-2A(\theta,\uparrow,\uparrow)\langle\underline{\mu}_1,\uparrow|\boldsymbol{L}\cdot\boldsymbol{S}|\underline{\mu}_2,\uparrow\rangle\langle\mu_2,\uparrow|\boldsymbol{L}\cdot\boldsymbol{S}|\mu_1,\uparrow\rangle$$
$$-2A(\theta,\downarrow,\downarrow)\langle\underline{\mu}_1,\downarrow|\boldsymbol{L}\cdot\boldsymbol{S}|\underline{\mu}_2,\downarrow\rangle\langle\mu_2,\downarrow|\boldsymbol{L}\cdot\boldsymbol{S}|\mu_1,\downarrow\rangle]. \tag{21}$$

The last two terms in (21), which do not reverse the spin, can be removed by considering an extra term due to $H = L_\zeta S_\zeta$. Using once again (19) and (20) we can write

$$\langle(L_\zeta S_\zeta)^2\rangle = \sum_{\mu_1,\underline{\mu}_1,\sigma_1} n_{\mu_1,\underline{\mu}_1,\sigma_1}\langle\underline{\mu}_1|(L_\zeta S_\zeta)^2|\mu_1\rangle$$
$$= \Delta E_{\rm ex}\sum_{\theta} A(\theta,\sigma_1,\sigma_1)\langle\underline{\mu}_1|L_\zeta S_\zeta|\underline{\mu}_2\rangle\langle\mu_2|L_\zeta S_\zeta|\mu_1\rangle. \tag{22}$$

3.6. Physical model

Defining the abbreviated notation

$$a(\sigma_1,\sigma_2) \equiv \sum_{\theta} A(\theta,\sigma_1,\sigma_2)\langle\underline{\mu}_1,\sigma_1|\boldsymbol{L}\cdot\boldsymbol{S}|\underline{\mu}_2,\sigma_2\rangle\langle\mu_2,\sigma_2|\boldsymbol{L}\cdot\boldsymbol{S}|\mu_1,\sigma_1\rangle \tag{23}$$

where we recall that the first spin index refers to that of the occupied level and the second spin index to that of the unoccupied level, we collect, for ease of comparison, the different

terms as

$$\delta E = -\xi^2[a(\uparrow,\uparrow) + a(\downarrow,\downarrow) - a(\uparrow,\downarrow) - a(\downarrow,\uparrow)] \tag{24}$$

$$\hat{\boldsymbol{S}} \cdot \langle \boldsymbol{L} \rangle \equiv \hat{\boldsymbol{S}} \cdot [\langle \boldsymbol{L}^{\uparrow} \rangle + \langle \boldsymbol{L}^{\downarrow} \rangle] = -4\xi[a(\uparrow,\uparrow) - a(\downarrow,\downarrow)] \tag{25}$$

$$\hat{\boldsymbol{S}} \cdot \langle \boldsymbol{T} \rangle \approx -\tfrac{2}{7}\hat{\boldsymbol{S}} \cdot \langle \boldsymbol{Q} \rangle \cdot \hat{\boldsymbol{S}} = \tfrac{2}{21}\Delta E_{\mathrm{ex}}[-2a(\uparrow,\uparrow) - 2a(\downarrow,\downarrow) + a(\uparrow,\downarrow) + a(\downarrow,\uparrow)] \tag{26}$$

$$\langle (L_\zeta S_\zeta)^2 \rangle = \Delta E_{\mathrm{ex}}[a(\uparrow,\uparrow) + a(\downarrow,\downarrow)]. \tag{27}$$

Since a theoretical model is as good as its physical picture, it is instructive to visualize the different terms with the help of the virtual excitations introduced in figure 1. Equation (24) shows that the energy decreases in the presence of excitations that conserve the spin, but increases for excitations that reverse the spin. Therefore, the easy direction of magnetization will be in the direction that provides the largest opportunity for 'ferromagnetic' excitations. It is clear from (24) that the energy is invariant for time reversal, i.e. δE does not change when all spin directions are reversed.

The projected orbital moment, $\hat{\boldsymbol{S}} \cdot \langle \boldsymbol{L} \rangle$, in (25) contains only excitations which conserve the spin. Due to time reversal symmetry the orbital moment changes sign when all spin directions are reversed. Comparison with the MAE in (24) shows that the orbital moment operator can only account for the ferromagnetic excitations, and moreover that it gives the opposite sign for spin up compared to spin down electrons. Therefore, the MAE cannot simply be taken proportional to the projected orbital moment. Only in the case that $a(\downarrow,\downarrow)$ is the dominant term, i.e. for a 'hard' ferromagnet, we can safely assume that the easy-magnetization axis is along the direction of the maximum orbital moment.

The magnetic dipole term, $\hat{\boldsymbol{S}} \cdot \langle \boldsymbol{T} \rangle$, in (26) contains both spin conserved and spin-flip terms, which have opposite sign with respect to each other. Only the quadrupole-induced part of the spin anisotropy has been taken into account, because the spin–orbit-induced part of the spin anisotropy is small in 3d transition metals. Since the quadrupole moment is invariant for time reversal, (21) does not change sign when the spin directions are reversed. Finally, the squared diagonal spin–orbit interaction in (27) conserves the spin in the excitation. It shares this property with the orbital moment; however, the latter reverses in sign for opposite spin directions.

Comparison of (24)–(27) gives the total MAE as

$$\begin{aligned}\delta E &\approx -\frac{1}{4}\xi \hat{\boldsymbol{S}} \cdot [\langle \boldsymbol{L}^{\downarrow} \rangle - \langle \boldsymbol{L}^{\uparrow} \rangle] + \frac{\xi^2}{\Delta E_{\mathrm{ex}}}\left[\frac{21}{2}\hat{\boldsymbol{S}} \cdot \langle \boldsymbol{T} \rangle + 2\langle (L_\zeta S_\zeta)^2 \rangle\right] \\ &\equiv E_L^{\downarrow} + E_L^{\uparrow} + E_T + E_{LS}.\end{aligned} \tag{28}$$

This conjecture forms the key result of our paper.

4. Discussion

4.1. Angular dependence

The angular dependence of δE, $\langle \boldsymbol{L} \rangle$ and $\langle \boldsymbol{T} \rangle$ is constrained by the symmetry of the crystalline field [3, 17, 18]. We briefly discuss here the angular dependence of the ground state magnetic moments. Equation (16) can be written in the form

$$\langle \boldsymbol{L}^{\downarrow(\uparrow)} \rangle = \boldsymbol{R}^{\downarrow(\uparrow)} \cdot \hat{\boldsymbol{S}} \tag{29}$$

with $\boldsymbol{R}$ a Cartesian tensor. In matrix form (using the Einstein notation) this gives $L_i = R_{ij}\hat{S}_j$, where $i, j \in \{x, y, z\}$, and similarly (2) gives $T_i = -\frac{2}{7}Q_{ij}\hat{S}_j$. In C_{2v} and higher symmetry the angular dependence of the vectors $\boldsymbol{L}$ and $\boldsymbol{T}$ is simply $K_0 + K_1 \sin^2 \nu$,

where $\nu = \angle\hat{\boldsymbol{S}}, \hat{\boldsymbol{z}}$. The remaining term E_{LS} in (28) is independent of the spin direction and gives an energy shift.

4.2. Measurement with magnetic x-ray dichroism

The importance of the conjecture relating the MAE to the orbital moment and magnetic dipole term is that these quantities can—in principle—be measured in an element-specific way using magnetic circular x-ray dichroism (MCXD), which is the difference between the x-ray absorption spectra with the light helicity vector parallel and antiparallel to the magnetization direction [36, 38].

The MAE is obtained by taking the magnetization along the different principal axes, e.g. for the contribution of the orbital moment term we have in C_{2v} and higher symmetry

$$\hat{S}_z \cdot \langle \boldsymbol{L} \rangle - \hat{S}_x \cdot \langle \boldsymbol{L} \rangle = R_{zz} - R_{xx} \tag{30}$$

where the R are found from the MCXD sum rules. For convenience we also define the isotropic and anisotropic part of the orbital moment

$$L^{(0)} \equiv \tfrac{1}{3}(R_{zz} + R_{xx} + R_{yy}) \tag{31}$$

$$L^{(2)} \equiv \tfrac{1}{3}(2R_{zz} - R_{xx} - R_{yy}). \tag{32}$$

In MCXD, sum rules give the value of the moments $\boldsymbol{L}$, $\boldsymbol{S}$ and $\boldsymbol{T}$ projected onto $\hat{\boldsymbol{P}}$, which is a unit vector pointing along the propagation direction of the circularly polarized light [22]. The projected orbital moment is obtained from the integrated $L_{2,3}$ dichroism signal and the projected effective spin moment is obtained from the weighted difference over the spin–orbit-split L_2 and L_3 core levels

$$\hat{\boldsymbol{P}} \cdot \langle \boldsymbol{L} \rangle = -\tfrac{4}{3}(A_3 + A_2)C \tag{33}$$

$$\hat{\boldsymbol{P}} \cdot \langle \boldsymbol{S}_{\rm eff} \rangle \equiv \hat{\boldsymbol{P}} \cdot [\langle \boldsymbol{S} \rangle + \tfrac{7}{2}\langle \boldsymbol{T} \rangle] = (A_3 - 2A_2)C \tag{34}$$

where C is a constant which depends on the number of holes and $A_{2,3}$ is the integrated MCXD signal at the $L_{2,3}$ edge. The values of the ground state moments can be obtained per valence d hole by using the isotropic spectrum for the normalization, since the integrated signal of the latter is proportional to the number of d holes [22]. Unfortunately, $\langle \boldsymbol{L}^{\uparrow} \rangle$ and $\langle \boldsymbol{L}^{\downarrow} \rangle$ cannot be measured separately. Their relative contributions can be estimated using theoretical models, such as band structure calculations. It has also been shown that this information is contained in the first spectral moment of the MCXD spectra [39, 40].

In an anisotropic medium away from the principal axes the vectors $\boldsymbol{L}$ and $\boldsymbol{T}$ are not collinear with $\hat{\boldsymbol{S}}$. For the orbital moment we measure

$$\hat{\boldsymbol{P}} \cdot \langle \boldsymbol{L} \rangle = \hat{\boldsymbol{P}} \cdot \boldsymbol{R} \cdot \hat{\boldsymbol{S}} = R_{zz} \cos\nu \cos\gamma + R_{xx} \sin\nu \sin\gamma \tag{35}$$

where $\nu = \angle\hat{\boldsymbol{S}}, \hat{\boldsymbol{z}}$ and $\gamma = \angle\hat{\boldsymbol{P}}, \hat{\boldsymbol{z}}$. When the applied magnetic field is strong enough to saturate the sample ($\hat{\boldsymbol{P}} \| \hat{\boldsymbol{S}}$), (35) simplifies to

$$\hat{\boldsymbol{P}} \cdot \langle \boldsymbol{L} \rangle = R_{zz} \cos^2\nu + R_{xx} \sin^2\nu = L^{(0)} + \tfrac{1}{2}(3\cos^2\nu - 1)L^{(2)}. \tag{36}$$

A interesting and recent addition to the dichroic measurements is transverse magnetic circular x-ray dichroism (TMCXD). Here, one makes use of the competition between the crystal field interaction and the spin–orbit coupling to measure the anisotropy in the ground state moments [41–43]. When the spins are forcefully aligned along a non-symmetry direction by a saturating external magnetic field, the spin–orbit coupling tries to align $\boldsymbol{L}$ parallel to $\boldsymbol{S}$, whereas the crystal field prefers an alignment of the orbital moment along the easy direction of magnetization, which is along a principal axis of the periodic lattice.

Consequently, $\boldsymbol{L}$ is no longer collinear with $\boldsymbol{S}$, and has a component perpendicular to $\boldsymbol{S}$ which can serve as a direct measure for the anisotropy in the orbital magnetic moment. This transverse orbital component can be obtained directly by applying the sum rules to the TMCXD spectrum, which is thus measured with a saturating magnetic field perpendicular to the photon helicity vector. In this transverse geometry ($\hat{\boldsymbol{P}} \perp \hat{\boldsymbol{S}}$) we measure

$$\hat{\boldsymbol{P}} \cdot \langle \boldsymbol{L} \rangle = \tfrac{1}{2}(R_{zz} - R_{xx}) \sin 2\nu = \tfrac{3}{4} \sin 2\nu \, L^{(2)} \tag{37}$$

which is thus directly proportional to the orbital magnetic anisotropy. Likewise, the transverse geometry enables us to separate the magnetic dipole term, $\boldsymbol{T}$, describing the anisotropy of the spin distribution, from the isotropic spin magnetic moment, $\boldsymbol{S}$ [41].

4.3. Relative magnitudes of E_L and E_T

The value of $E_L^{\downarrow\,(\uparrow)}$ depends strongly on the filling of the spin subband. Because the denominator in (11) contains the energy difference $\varepsilon_2 - \varepsilon_1$ between states which are located below and above the Fermi level the anisotropy is essentially determined by the states near the Fermi level. Since for E_L there are no cross terms between the two spin directions, we can look at each spin band separately. The matrix elements of $\boldsymbol{L}$ are given in table 1 for the crystal-field-split d states. Those for p states are given for comparison in table 2. Diagonal matrix elements are zero, because the crystal field wavefunctions have no imaginary part, so that only the non-diagonal matrix elements which have $\Delta m = 0, \pm 1$ can be non-zero.

Table 1. Matrix elements $\langle \mathrm{d}_i | \hat{\boldsymbol{e}} \cdot \boldsymbol{L} | \mathrm{d}_j \rangle$ with $L_z = -\mathrm{i}(x\partial/\partial y - y\partial/\partial x)$ and cyclic.

	$\langle zx\|$	$\langle yz\|$	$\langle xy\|$	$\langle x^2 - y^2\|$	$\langle 3z^2 - r^2\|$
$\|zx\rangle$	0	$-\mathrm{i}\hat{e}_z$	$\mathrm{i}\hat{e}_x$	$-\mathrm{i}\hat{e}_y$	$\mathrm{i}\sqrt{3}\hat{e}_y$
$\|yz\rangle$	$\mathrm{i}\hat{e}_z$	0	$-\mathrm{i}\hat{e}_y$	$-\mathrm{i}\hat{e}_x$	$-\mathrm{i}\sqrt{3}\hat{e}_x$
$\|xy\rangle$	$-\mathrm{i}\hat{e}_x$	$\mathrm{i}\hat{e}_y$	0	$2\mathrm{i}\hat{e}_z$	0
$\|x^2 - y^2\rangle$	$\mathrm{i}\hat{e}_y$	$\mathrm{i}\hat{e}_x$	$-2\mathrm{i}\hat{e}_z$	0	0
$\|3z^2 - r^2\rangle$	$-\mathrm{i}\sqrt{3}\hat{e}_y$	$\mathrm{i}\sqrt{3}\hat{e}_x$	0	0	0

Table 2. Matrix elements $\langle \mathrm{p}_i | \hat{\boldsymbol{e}} \cdot \boldsymbol{L} | \mathrm{p}_j \rangle$.

	$\langle x\|$	$\langle y\|$	$\langle z\|$
$\|x\rangle$	0	$\mathrm{i}\hat{e}_z$	$-\mathrm{i}\hat{e}_y$
$\|y\rangle$	$-\mathrm{i}\hat{e}_z$	0	$\mathrm{i}\hat{e}_x$
$\|z\rangle$	$\mathrm{i}\hat{e}_y$	$-\mathrm{i}\hat{e}_x$	0

The value of E_T depends on both the quadrupole moment and the spin–orbit coupling in the ground state. Since the latter is small, its main effect is to induce an alignment between spin and orbital. The quadrupole moment $Q_{zz} = l_z^2 - \frac{1}{3}l(l+1)$ is diagonal in $\mathrm{C_{2v}}$ and higher symmetries. This gives $Q_{zz} = 2$ for the xy and $x^2 - y^2$ states, $Q_{zz} = -1$ for the yz and xz states and $Q_{zz} = -2$ for the $3z^2 - r^2$ state. A positive value of Q_{zz} means that high values of $|m|$ are occupied which makes the change distribution flat in the xy plane and the preferred magnetization perpendicular to the plane. For a negative value the charge distribution is elongated along the z axis and the preferred magnetization is in plane. Spin–orbit interaction couples Q_{zz} to the spin direction. In this way the anisotropy of the spin influences the easy direction of magnetization.

In ferromagnetic 3d metals, such as iron where $\xi \simeq 0.05$ eV and $\Delta E_{\rm ex} = \sim 3$ eV, E_L is about an order of magnitude larger than E_T. In 4d metals the spin–orbit constant increases along the series from $\sim$0.03 to $\sim$0.2 eV and in 5d metals from $\sim$0.1 to $\sim$0.5 eV, so that E_T becomes important. Thin films and clusters of the 4d metals Ru, Rh and Pd show induced magnetism. Calculations show that the 5d metals Ir and Pt, in the monolayer range, are magnetic when grown on Ag. However, no experiment has displayed any kind of magnetism yet and more realistic calculations have suggested that spin–orbit effects kill the magnetic moment [44].

4.4. Phase diagram

For a start consider two states with exactly the same orbital character but with opposite spin. The expectation value of the orbital magnetic moment reverses with the spin direction, so that for these two states $\langle \boldsymbol{L}^{\downarrow} \rangle = -\langle \boldsymbol{L}^{\uparrow} \rangle$. However, $\langle \boldsymbol{L}^{\downarrow} \rangle$ and $\langle \boldsymbol{L}^{\uparrow} \rangle$ have opposite signs in (28), so that the MAE is independent of the spin, i.e. $E_L \equiv E_L^{\downarrow} = E_L^{\uparrow}$. Since also E_T is independent of the spin, the dependence as a function of band filling is the same for majority and minority spin band. Therefore, the dependence of the MAE on the ratio $R = E_T/(E_T + E_L)$ as a function of the d band filling can be captured in just a single diagram.

We will illustrate the competition between E_L and E_T by the example of an ultrathin film extending in the xy plane. Figure 2 shows the diagram for the situation where the xy and $x^2 - y^2$ orbitals have the strongest bonding, resulting in well separated bonding and anti-bonding orbitals, which as a function of band filling will be filled first and last, respectively. The $3z^2 - r^2$ orbitals lie mainly along the layer normal and form δ bondings, which exhibit the weakest dispersion.

The variation of the MAE due to E_L as a function of the number of electrons, n, in the subband, can be found along the line $R = 0$ in figure 2. Its dependence has been given by Bruno [16] and Wang *et al* [11] and can be found with the help of table 1. Light (dark) shaded regions correspond to negative (positive) values of the MAE favouring in-plane (perpendicular) magnetization. The sign of E_L changes for $1/3$ and $2/3$ filled bands. An almost filled or empty spin band gives a negative value of E_L, whereas a half filled band gives a positive value. This picture is of course oversimplified: the reality depends also on the details of the electronic structure. The behaviour as a function of n is very different for the spin-flip contribution, E_T, displayed along the line $R = 1$, which shows a sign change when the subband is half filled. Filling the $3z^2 - r^2$ state makes the value of E_T positive, whereas filled xy and $x^2 - y^2$ states make it negative. Thus the E_L and E_T contributions have the same effect on the MAE for an almost empty spin band, but give the opposite effect when the spin band is almost filled. Therefore, in a nearly filled band metal which has strong bonds in the xy plane, PMA is only expected when E_T is large, such as for 4d and 5d metals.

Figure 2 shows that for dominant E_L there is a broad region centred around $n = 2.5$ with a strong preference for PMA. If we assume that all the holes are in the minority band, this would indeed be in agreement with the experimental observations for the magnetic anisotropy of 3d transition metal systems. Ferromagnetic Fe- and Co-based multilayers and thin films often favour PMA [45], whereas Ni systems are usually in-plane magnetized. However, such a single-band picture is too simple, since in reality there are also holes in the majority band. Both sum rule and line shape analysis of MCXD spectra give spin polarizations $P = (n_{\uparrow} - n_{\downarrow})/(n_{\uparrow} + n_{\downarrow}) = 2S/n_d$ of about 0.55, 0.65 and 0.7 for Fe, Co and Ni metal, respectively [39, 40]. In a nearly filled d metal, such as Ni, the presence of holes

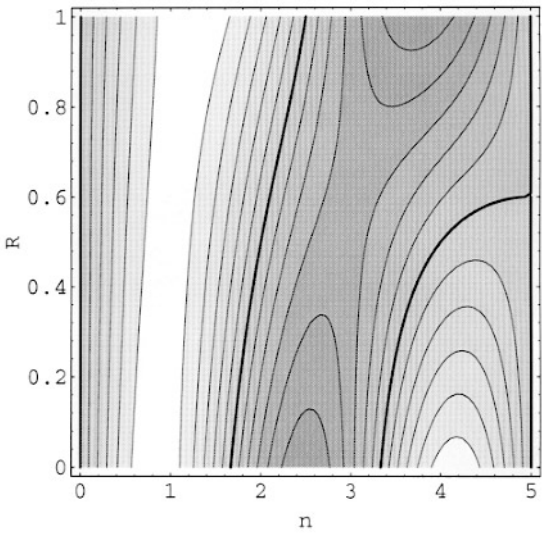

Figure 2. Dependence of the MAE on the ratio $R = E_T/(E_T + E_L)$ as a function of the d band filling where n is the number of electrons in the spin subband. When the strongest bonds are in the xy plane, the light (dark) shaded regions correspond to negative (positive) values of the MAE favouring an in-plane (perpendicular) magnetization. Zero contours have been marked by a thicker line. The diagram is valid for both spin bands, even though the expection values of their orbital moments are opposite in sign. When the strongest bonds are in the z direction, light and dark shades have to be reversed.

in the majority band with opposite orbital moment will decrease the total orbital moment per hole, while the MAE per hole remains the same (cf figure 2). For materials where the majority band is more than 2/3 filled, and the minority band is between 1/3 and 2/3 filled, as is expected for Fe and Co metal, $L^{\downarrow}$ and $L^{\uparrow}$ will have the same sign (cf figure 2). This results in a large orbital moment, but a reduced MAE. This is in agreement with recent results which indicate that the MAE is smaller than expected from the measured orbital moment when it is assumed that the majority band is completely filled [43]. Conversely, one might also encounter situations where the total orbital moment is very small, but the MAE is large, which can occur e.g. for Mn d^5.

So far we have described only the case where the strongest bonds are in the xy plane. In systems, where the interface means that the $3z^2 - r^2$ orbital has the strongest bonding, the situation presented above is reversed. Figure 2 still applies, but light and dark shades should be reversed with the result that Co and Fe systems will now display a strong in-plane magnetization, whereas Ni can show PMA. Note that the strain can dictate which bondings are the strongest [46]. Finally, we should mention that in lower symmetries there can also be a strong anisotropy within the plane of the film [47].

5. Conclusions

The recent renaissance in magnetic research following the discovery of magnetic phenomena associated with artificially made thin films of transition metals, many of them specifically based on anisotropic properties, such as perpendicular magnetic anisotropy and giant magneto-resistance, made it timely to investigate the validity of the Bruno model [16]

and the importance of other possible contributions, such as the magnetic dipole term. The magnetocrystalline anisotropy energy can be expressed in terms of the projected magnetic moments $\hat{\boldsymbol{S}} \cdot \langle \boldsymbol{L} \rangle$ and $\hat{\boldsymbol{S}} \cdot \langle \boldsymbol{T} \rangle$. The contribution due to the orbital magnetization depends most strongly on the character of the states near the Fermi level. In a proper analysis of the MAE the orbital moments of the spin up and spin down bands have to be taken separately into account. Only when the majority band is completely filled will the MAE be proportional to the anisotropic orbital magnetic moment. The magnetic dipole term accounts for the spin-flip contributions in the MAE. Its influence in 3d metals is much weaker than the contribution due to the orbital moment, since it scales with the ratio of the spin–orbit coupling over the exchange interaction. With the strongest bands in the xy plane, and the orbital contribution as the dominant term, we find from the E_L, E_T phase diagram that Fe and Co thin films are the most likely candidates for PMA, whereas Ni will be usually in-plane magnetized. The expectation values of the orbital moment and the magnetic dipole term can be obtained from MCXD using the sum rules. It is less straightforward to obtain the contributions of the orbital moments separated by spin, but line shape analysis can open up new avenues [39, 40].

References

[1] Gradmann U and Müller J 1968 *Phys. Status Solidi* **27** 313
[2] Heinrich B and Bland J A C (ed) 1994 *Ultrathin Magnetic Structures* (Berlin: Springer)
[3] Bruno P 1993 *Physical Origins and Theoretical Models of Magnetic Anisotropy* (Ferienkurse des Forschungszentrums Jülich, Jülich)
[4] Bander M and Mills D L 1988 *Phys. Rev.* B **38** 12 015
[5] Draaisma H J G and de Jonge W J M 1988 *J. Appl. Phys.* **64** 3610
[6] van Vleck J H 1937 *Phys. Rev.* **52** 1178
[7] Brooks H 1940 *Phys. Rev.* **58** 909
[8] Daalderop G H O 1994 *PhD Thesis* University of Delft
[9] Gay J G and Richter R 1994 *Ultrathin Magnetic Structures* ed B Heinrich and J A C Bland (Berlin: Springer) p 21
[10] Gay J S and Richter R 1987 *J. Appl. Phys.* **61** 3362
[11] Wang D S, Wu R and Freeman A J 1993 *Phys. Rev. Lett.* **70** 869
Wang D S, Wu R and Freeman A J 1993 *Phys. Rev. Lett.* **71** 2166
[12] Daalderop G H O, Kelly P J and Schuurmand M F H 1993 *Phys. Rev. Lett.* **71** 2165
[13] van der Laan G 1991 *J. Phys.: Condens. Matter* **3** 7443
van der Laan G and Kirkman I W 1992 *J. Phys.: Condens. Matter* **4** 4189
[14] Callen E R and Callen H B 1963 *Phys. Rev.* **129** 578
Callen E R and Callen H B 1965 *Phys. Rev.* **139** A455
[15] Jensen J and Mackintosh A R 1991 *Rare Earth Magnetism* (New York: Oxford University Press)
[16] Bruno P 1989 *Phys. Rev.* B **39** 865
Bruno P 1989 *PhD Thesis* Orsay
[17] Abate E and Asdente M 1965 *Phys. Rev.* **140** A1303
[18] Takayama H, Bohnen K P and Fulde P 1976 *Phys. Rev.* B **14** 2287
[19] Cinal M, Edwards D M and Mathon J 1994 *Phys. Rev.* B **50** 3754
Cinal M, Edwards D M and Mathon J 1995 *J. Magn. Magn. Mater.* **140** 681
[20] Wang D S, Wu R and Freeman A J 1993 *Phys. Rev.* B **47** 14 932
[21] van der Laan G and Thole B T 1995 *J. Phys.: Condens. Matter* **7** 9947 appendix A
[22] van der Laan G 1996 *J. Magn. Magn. Mater.* **156** 99
[23] Collins S P, Laundy D, Tang C C and van der Laan G 1995 *J. Phys.: Condens. Matter* **7** 9325
[24] van der Laan G and Thole B T 1996 *Phys. Rev.* B **53** 14 458
[25] Néel L 1954 *J. Physique Radium* **15** 376
[26] Krakauer H, Freeman A J and Wimmer E 1983 *Phys. Rev.* B **28** 610
[27] van der Laan G, Hoyland M A, Surman M, Flipse C F J and Thole B T 1992 *Phys. Rev. Lett.* **69** 3827
[28] Tischer M *et al* 1995 *Phys. Rev. Lett.* **75** 1602
[29] Dürr H A, van der Laan G, Vogel J, Panaccione G, Brookes N B, Dudzik E and McGrath R 1998 unpublished

[30] Hjortstam O, Trygg J, Wills J M, Johansson B and Eriksson O 1996 *Phys. Rev.* B **53** 9204
[31] van Vleck J H 1932 *Electric and Magnetic Susceptibilities* (Oxford: Oxford University Press)
[32] Abragam A and Bleaney B 1970 *Electron Paramagnetic Resonance of Transition Ions* (Oxford: Oxford University Press)
[33] Mabbs F E and Machin D J 1973 *Magnetism and Transition Metal Complexes* (London: Chapman and Hall)
[34] van der Laan G 1997 *Electron Spectrosc. Relat. Phenom.* **86** 57
[35] Kanamori J 1963 *Anisotropy and Magnetostriction of Ferromagnetic and Antiferromagnetic Materials (Magnetism 1)* ed G T Rado and H Suhl (New York: Academic)
[36] Carra P, Thole B T, Altarelli M and Wang X 1993 *Phys. Rev. Lett.* **69** 2307
[37] Stöhr J and König H 1995 *Phys. Rev. Lett.* **75** 3748
Dürr H A, van der Laan G and Thole B T 1996 *Phys. Rev. Lett.* **76** 3464
[38] Thole B T, Carra P, Sette F and van der Laan G 1992 *Phys. Rev. Lett.* **68** 1943
[39] van der Laan G 1997 *Phys. Rev.* B **55** 8086
[40] van der Laan G 1997 *J. Phys.: Condens. Matter* **9** L259
[41] Dürr H A and van der Laan G 1996 *Phys. Rev.* B **54** R760
[42] Dürr H A and van der Laan G 1997 *J. Appl. Phys.* **81** 5355
[43] Dürr H A, Guo G Y, van der Laan G, Lee J, Lauhoff G and Bland J A C 1997 *Science* **277** 213
[44] Dreyssé H and Demangeat C 1997 *Surf. Sci. Rep.* **28** 67
[45] de Jonge W J M, Bloemen P J H and den Broeder F J A 1994 *Ultrathin Magnetic Structures* ed B Heinrich and J A C Bland (Berlin: Springer) p 65
[46] Lee J, Lauhoff G, Tselepi M, Hope S, Rosenbusch P, Bland J A C, Dürr H A, van der Laan G, Schillé J P and Matthew J A D 1997 *Phys. Rev.* B **55** 15 103
[47] Pastor G M, Dorantes-Dávila J, Pick S and Dreyssé H 1995 *Phys. Rev. Lett.* **75** 326
Rodriguez-Lopez J L, Dorantes-Davila J and Pastor G M 1998 *Phys. Rev.* B **57** 1040